THE POTENTIAL OF THERMALLY CONDUCTIVE POLYMER COMPOSITES REGARDING CRYSTALLIZATION FOULING MITIGATION

*H. Kiepfer[1], H.-J. Bart[1], P. Stannek[2], M. Kuypers[2], M. Grundler[2]

[1]Laboratory of Reaction and Fluid Process Engineering, TU Kaiserslautern, 67663 Kaiserslautern, Germany
E-mail: hendrik.kiepfer@mv.uni-kl.de; bart@mv.uni-kl.de
[2] Zentrum für BrennstoffzellenTechnik (ZBT) GmbH, 47057 Duisburg, Germany

ABSTRACT

The fouling kinetics and amount of calcium sulfate and calcium carbonate, respectively, on different polypropylene/graphite composites in a flat plate heat exchanger are determined and compared to the reference material stainless-steel. For a straight evaluation of the fouling susceptibility of the materials the formation of bubbles on the materials is considered by optical imaging or excluded by a degasser. The results are interpreted using surface free energy and roughness of the surfaces.

The results show that when bubble formation is avoided, the polymer composites have a very low fouling tendency compared to stainless steel. This is particularly the case when turbulent flows are present or when sandblasted specimen are used. Sandblasting also continues to increase heat transfer compared to untreated samples by increasing thermal conductivity and creating local turbulences. Depending on the test conditions, the fouling resistance formed on the stainless-steel surface is an order of magnitude greater than on the polymer composites. In addition, the fouling layers adhere only weakly to the composites, which indicates an easy cleaning in place after the formation of deposits.

INTRODUCTION

Fouling is commonly defined as the deposition of undesired substances with usually low thermal conductivity on heat transfer surfaces, which result in additional heat transfer resistance as well as increased pressure loss [1]. The consequences are increased operating and maintenance costs [2]. In order to compensate the reduced heat transfer rates, the required heat exchangers are oversized as a precaution, or a larger use of heating or cooling utilities is required.

In the context of the energy saving and CO_2 reduction, both approaches are disadvantageous. Another cost factor arises in the environment of corrosive media, such as seawater, acids, bases, electroplating and pickling baths. According to the state of the art heat exchangers made of expensive nonferrous and semi-precious metals or high-quality or high-priced stainless steels have to be used for these applications [3].

Compared to metals, polymers are less susceptible to corrosion and fouling, but have a low thermal conductivity below 0.5 W/mK [4] and poor mechanical properties. The disadvantage of low thermal conductivity can be compensated by manufacturing composite materials. Here polymers loaded with highly conductive particles such as graphite, which can increase the thermal conductivity up to 20 W/mK [5].

Although such polymer composites have been widely studied as heat transfer materials [6], there are few studies on their fouling susceptibility, especially for plate-like materials [7]. However, to evaluate the suitability of these materials as plate heat exchanger materials, which are used among other fields, in water treatment where crystallization fouling occurs [8], this is precisely the issue that needs to be addressed. Therefore, self-developed polypropylene-graphite composites are evaluated for suitability in this type of heat exchanger with respect to their susceptibility to crystallization fouling. Besides the influence of different salt species and wall temperatures, the influence of air bubbles on the surface is also discussed as they strongly influence fouling processes.

MATERIALS AND METHODS

Materials and preparation

The heat transfer materials investigated in this work are manufactured by the hydrogen and fuel cell center ZBT GmbH. For this purpose, highly filled graphite-polymer compounds are produced using a twin-screw or ring extruder. Subsequently, these compounds are processed in a mill to gain a homogeneous granulate of < 4 mm. The compound pellets are then transferred to a single-screw extruder as basis of the film extrusion. There, the compounds melt again and pass through a wide slot die (width

250 mm) with variable gap dimension to the calender. The gap dimension of the calender is variable adjustable between 0.2 mm and 25 mm and smoothes the surfaces of the melt.

To focus on the fouling susceptibility of the materials, the investigations are limited to two nearly identical polymer blends. This is legitimized by the fact that previous work showed that polymer and graphite grade had little effect on surface and thermal properties (primarily on the thermal conductivity [9]). Only sandblasting (sb) as post-treatment is considered and discussed here as it is a straightforward way to increase the thermal conductivity of the composites produced. After manufacturing, the materials have a thin polymer layer on the surface, which has a lower thermal conductivity than the core. Sandblasting removes this layer, which increases the thermal conductivity of the material by approx. 10% (see Table 1).

The naming of the developed composites is composed as follows: polypropylene grade (e.g., C143) - filler content in wt.%. The graphite used is a graphite with a D90 value of 45 μm (90 wt.% of particles smaller than 45 μm). Moreover, stainless steel 1.4571 (SS), a standard material in apparatus design is used as a benchmark. The wall thickness selected for all materials was 1 mm.

Material characterization

Since the crystal-surface interactions strongly depend on the energetic and topographic properties of the surface, these should be considered for the interpretation of the results of the fouling experiments. For this purpose, the surface free energies including polar and disperse fractions as well as the surface roughness of the investigated materials are determined. By means of a confocal microscope (μsurf Explorer, Nanofocus AG), 3D surface profiles are obtained from which various roughness parameters can be extracted and quantified according to EN ISO 25178. For the characterization of the topography of the materials, the mean arithmetic surface roughness is used as a parameter for this purpose. Compared to the line roughness it provides more accurate and reproducible results. The polar and diparamsperse fraction of the surface free energies are determined according to the OWRK method by measuring static contact angles (sessile drop method) [10,11]. This requires contact angle measurements with at least two liquids with known polar and disperse fractions of the surface tension. To increase the accuracy of the results, static contact angle measurements with four reference liquids (deionized water, ethylene glycol, DMSO, diiodomethane) were performed with an OCA 15 EC setup (Dataphysics). In addition to the surface properties, the surface temperature of the materials determines the fouling propensity. This results from the operating parameters (volume flows, inlet temperatures, …) in the heat exchangers, as well as the thermal conductivity of the materials investigated. Consequently, the thermal conductivities of the self-produced materials were determined by laser flash analysis as listed in Table 1 on the Laser Flash Apparatus 457 (Netzsch).

Table 1: Thermal properties of the materials.

Material	λ / W/mK
SS	15
C143-75	1.64
C143-75-sb	1.80
C145-80	1.96

Experimental set up

The fouling experiments were carried out at various operating conditions in the screening apparatus shown schematically in Figure 1. The setup contains a vertically oriented interchangeable test section (4). Two plate heat exchanger test cells are utilized, which are both operated in counter current flow. The first test cell (HX1) has a rectangular heat transfer surface of 144 cm². To avoid vortex formation and thus locally strong shear forces during the fouling experiments, the inlets are aligned longitudinally to the heat transfer surface. In addition, flow diffusers are located at the inlets and outlets to ensure a uniform flow over the heat transfer surface. However, the flow entering HX1 can neither be assumed as hydrodynamically nor thermally fully developed. The same applies to the second parallel test cell (HX2), which has a heat transfer area of 32 cm². The liquid inlets and outlets are aligned transversely to the heat transfer surface, a usual for plate heat exchangers. Although vortex formation cannot be suppressed in this way, this represents a more realistic setup.
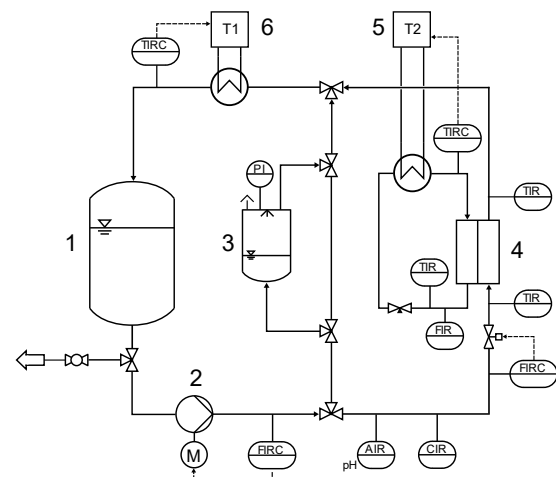

Figure 1: Process flowchart of the experimental set-up. (1) storage tank. (2) pump. (3) degasser. (4) heat exchanger test cell. (5) thermostat for heating circuit. (6) thermostat for bulk temperature control.

The sample material acts as a heat transfer wall and separates the cold liquid (salt solution) from the

hot liquid (hot water). The heating side of the test section is made of polyoxymethylene and is additionally insulated to ensure almost adiabatic conditions. The solution side is made of polymethylmethacrylat to allow visual monitoring of the fouling process and possible bubble formation. Temperature sensors (Pt100 1/3 DIN) were placed in the flow directly at the inlet and outlet of the test sections, where the temperature distribution and flow profiles are homogeneous. The volume flow rates of the fluids entering the heat exchanger, as well as their temperature, are controlled for constant test conditions. All relevant temperatures and volume flows are recorded transiently to guarantee an accurate energy balance. Using the energy balance for the calculation of the heat transfer rate $\dot{Q}$, the overall heat transfer coefficients U are calculated according to Eq. 1. The calculations of the heat transfer rate are based on the cold fluid, where energy losses are almost excluded, and a very accurate Coriolis flow meter is used (measuring accuracy of 0.1 %).

$$U = \frac{\dot{Q}}{A\Delta T_{lm}} \qquad (1)$$

As a result of crystallization fouling, the heat transfer rate changes with increasing test duration, providing a transient overall heat transfer coefficient U_f. The resulting fouling resistance R_f is then calculated according to Eq. 2 referring to the initial overall heat transfer coefficient U_0 of the clean surface.

$$R_f = \frac{1}{U_f} - \frac{1}{U_0} \qquad (2)$$

Experimental procedure

Prior to each experiment, the investigated polymer compound samples respectively the SS samples were cleaned with isopropanol and deionized water. The screening apparatus was cleaned several times with deionized water to ensure that there were no foreign ions left in the system. The feed solution for the $CaCO_3$-scaling tests is prepared by adding $CaCl_2 \cdot 2\,H_2O$ and $NaHCO_3$ to temperature-controlled deionized water, resulting in an initial pH value of about 7.7. For $CaSO_4$-scaling (that is not pH sensitive), the procedure is conducted with the salts Na_2SO_4 and $Ca(NO_3)_2 \cdot 4\,H_2O$. Regarding the measurement of the initial overall heat transfer coefficients, the data were recorded for 15 minutes after reaching a steady state before the addition of the second salt (fouling excluded). The bias uncertainties in the initial overall heat transfer coefficients were determined by calculating the 95 % confidence intervals according to Eq. 3, which are composed of the measurement uncertainties of the recorded temperatures ($T_{h,in}$, $T_{h,out}$, $T_{c,in}$, $T_{c,out}$) and the mass flow of the cold fluid.

$$B_U = \sqrt{\left[\sum_T \left(\frac{\partial U}{\partial T}B_T\right)^2 + \left(\frac{\partial U}{\partial \dot{m}_c}B_{\dot{m}_c}\right)^2\right]} \qquad (3)$$

The test period of the investigations was either adjusted to allow a sound conclusion on the fouling kinetics or to achieve an asymptotic fouling resistance. To accelerate the fouling processes, which can be achieved by high wall temperatures, laminar flow conditions were created on the cold fluid side (which contains the fouling salts) and turbulent flow conditions on the hot fluid side. In the experiments where bubble formation on the investigated surfaces should be suppressed, a vacuum spray-tube degasser (see Figure 1) was operated before the start of the experiments, which, according to the manufacturer, removes 90 % of the dissolved gases. This completely suppressed the formation of bubbles on the surface. Degassing of the fluid before the start of a fouling experiment is indicated subsequently by dg (degassed). The parameters of all performed fouling experiments are listed in Table 2.

Surface temperature calculation

To draw sound conclusions regarding the fouling processes investigated, knowledge of the surface temperature is crucial besides the surface properties. Since the surface temperatures were not controlled, but result from the selected operating parameters as well as material thickness and thermal conductivity, they were estimated as described below. The fluid temperature variation in the heat exchangers in flow direction x was calculated according to Eq. 4 & 5.

$$\frac{dT_c}{dx} = \frac{Uw}{\dot{m}c_p}(T_h - T_c) \qquad (4)$$

$$\frac{dT_h}{dx} = \frac{Uw}{\dot{m}c_p}(T_c - T_h) \qquad (5)$$

To calculate U, respectively the convective heat transfer coefficients h, Nusselt correlations for turbulent [12] and laminar flows [12,13] were applied. The relation in Eq. 6 was then used to calculate the wall temperatures, which are listed in Table 2.

$$\dot{Q} = \frac{T_h - T_{w,h}}{\frac{1}{h_h A}} = \frac{T_{w,c} - T_c}{\frac{1}{h_c A}} = \frac{T_h - T_c}{\frac{1}{UA}} \qquad (6)$$

Since there are various correlations for the calculation of convective heat transfer coefficients, these were selected to minimize the discrepancy between experiment and model. This procedure led to very small deviations between measured and calculated heat transfer rates for the HX1. These were on average 4 % but maximum 5.9 %.

Table 2: Operating parameters of the fouling experiments.

Exp. Nr.	Material	Test unit	Re_c	Re_h	$T_{c,in}$ / °C	$T_{h,in}$ / °C	$T_{w,0,calc}$ / °C	Salt	b_{salt} / mmol/kg
1	SS	HX1	500	3900	30	80	68.9	$CaSO_4$	25
2	C143-75	HX1	500	3900	30	80	-	$CaSO_4$	25
3	C143-75-dg	HX1	500	3900	30	80	60.9	$CaSO_4$	25
4	C143-75-sb	HX1	500	3900	30	80	61.6	$CaSO_4$	25
5	SS	HX1	500	3900	40	90	79.4	$CaSO_4$	25
6	C143-75	HX1	500	3900	40	90	-	$CaSO_4$	25
7	C143-75-dg	HX1	500	3900	40	90	71.1	$CaSO_4$	25
8	C143-75-sb	HX1	500	3900	40	90	71.7	$CaSO_4$	25
9	SS	HX2	500	5000	30	80	66.1	$CaSO_4$	25
10	C145-80	HX2	500	5000	30	80	58.7	$CaSO_4$	25
11	SS	HX2	500	5000	30	80	66.1	$CaCO_3$	3.5
12	C145-80	HX2	500	5000	30	80	58.7	$CaCO_3$	3.5

However, for the HX2, which shows flow conditions that are more difficult to describe, the maximum deviation is 14.6% and the average deviation is 9.3%. In addition, estimating the wall temperatures in the presence of air bubbles on the polymer composite surfaces (as discussed later) turns out to be almost impossible, since these represent a location-dependent, transient thermal resistance and strongly influence the flow regime at the surface. It can be expected, though, that higher wall temperatures will occur than on the SS surface with the same operating parameters.

Optical bubble detection

Under favorable conditions (e.g., if cavitation nuclei are present at the wall), bubbles can form and adhere on the heat transfer surface of the cold fluid side during the experiments. The gases dissolved in the fluid are present there in a supersaturated form due to the higher wall temperature compared to the bulk. In order to determine the degree of bubble coverage on the heat transferring surface, an optical image analysis is performed using an algorithm using functions of the Image Processing Toolbox of Matlab®. This generates binary images representing the bubble coverage on the surface as illustrated in Figure 2. The pictures were taken using a Nikon D5600 SLR camera.
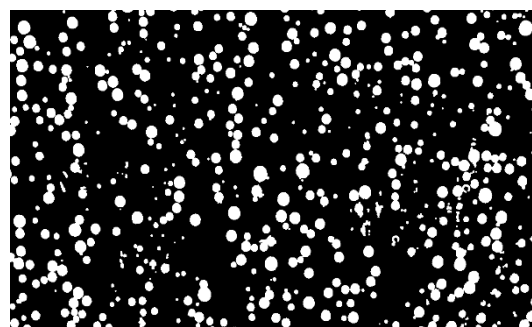

Figure 2: Binary image for bubble detection.

RESULTS AND DISCUSSION

Bubble influence on the fouling resistance

If air bubbles form on the heat transfer surface during a fouling experiment, there are two effects that influence the transient fouling resistance. The first issue is the development of an apparent fouling resistance that is not accompanied by deposition. This effect is illustrated in Figure 3. In fact, this is a thermal resistance due to the formation of air bubbles on the heat exchanger surface. Henceforth referred to as R_b.
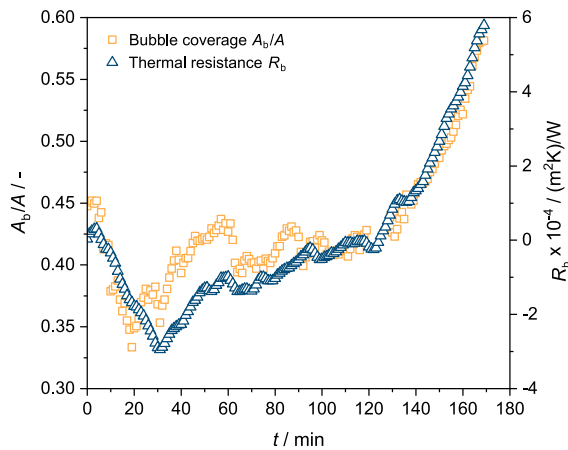
Figure 3: Influence of surface bubble coverage on the thermal resistance. Exp. 2.

Particularly the addition of salt at the beginning of the experiments leads to a supersaturation of the gases in the solution in proximity to the hot sample surfaces. Consequently, many bubbles form on the surface under investigation. To put this into perspective, it must be added that this behavior was only observed in the case of the untreated polymer composites for the HX1.

Almost no bubbles formed on the SS surface and on the sandblasted polymer composite surface they did not adhere. Hence, no change in the overall heat transfer coefficient by avoiding air bubbles (degassing) could be observed, which is why the optical evaluation for the fouling tests was not carried out with these materials. The same applies to the HX2. Even if the Reynolds numbers indicate laminar flow, the arrangement of the inlets causes local turbulence, which prevents the formation of bubbles. The magnitude of the influence of bubble coverage on the polymer composite is shown by Figure 4. The heat transfer coefficient at the beginning of the fouling test is up to 40% lower in the presence of bubbles (C143-75) than in the absence of bubbles (C143-75-dg and C143-75-sb, respectively). Consequently, more gas residues are present at the surface of the polymer composites, which act as initiators for the formation of bubbles. This so-called heterogeneous bubble formation depends strongly on the surface properties. Rough hydrophobic surfaces (such as the polymer composites used, see Table 4) nucleate bubbles easily even at low supersaturations, while hydrophilic or even smooth hydrophobic surfaces (such as SS) nucleate bubbles only at exceptionally large supersaturations [14,15].
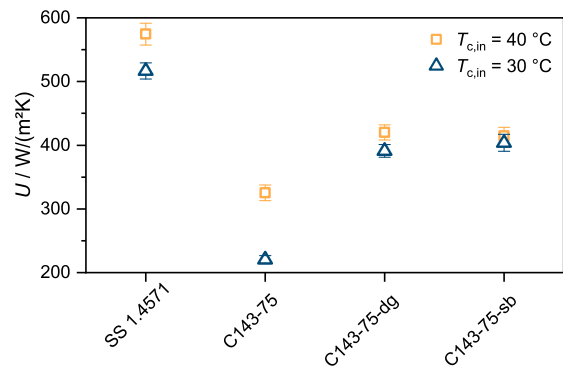

Figure 4: Overall heat transfer coefficients U_0 at the beginning of the fouling experiments in HX1.

In the case of the sandblasted material, which has a superhydrophobic surface due to its high roughness (see Table 4), bubbles do form, but these bead off in a similar way to the lotus effect and do not adhere [16]. As a result, the bubble coverage of the surface is so low that it has no measurable impact on the overall heat transfer coefficient.

The second issue that arises when air bubbles form on heat transfer surfaces is an enhanced formation of deposits, as can be seen in Figure 5. In the case of non-sandblasted polymer composite, two fundamentally different results are obtained depending on whether the test solution was previously degassed or not. The fouling resistance that occurs after 60 hours, when the test solution has not been degassed (dg) previously, is approximately a factor of 20 greater compared to degassed solution.
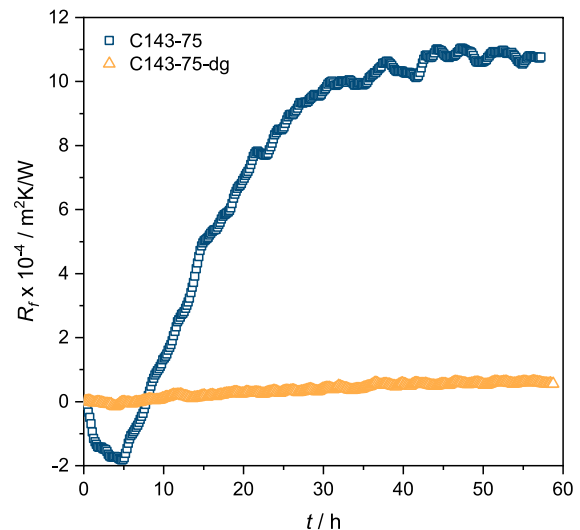

Figure 5: Influence of bubble formation on the fouling resistance. Exp. 2+3.

In this case, the heat transferring surface was almost completely covered with air bubbles, that could not be removed by the existing laminar flow and buoyancy forces. The consequence of such gas accumulation has already been discussed in the literature and has a severe effect on the fouling

process [17]. When gas bubbles grow on active nucleation sites on the heat transfer surface, the temperature beneath the gas bubbles and in the vicinity of the heat transfer surface increases. Consequently, there is a higher supersaturation at the boundary layer, which enhances the deposition of the salts. The structure of the deposits also changes considerably as evident in Figure 6. The bubble structure is clearly recognizable there and differs from the classical crystal structures.
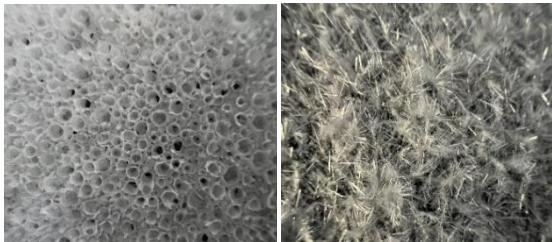

Figure 6: Influence of the presence of bubbles in the fouling process on the crystal structure formed; (l) bubbles, Exp. 2 (r) no bubbles, Exp. 5.

In order to avoid fouling on the composites investigated here and hence make them competitive with the reference material SS, adherent air bubbles on the surfaces must be avoided. The possibilities to achieve this are degassing of the fluids containing the substances causing fouling, prevention by surface adjustment or hydrodynamic adjustment to remove the bubbles. From a technical point of view, only the two proposals mentioned last are suitable.

Fouling kinetics and quantity

Figure 7 and Figure 8 show the results of the fouling tests in HX1 for two different fluid temperatures and $CaSO_4$ fouling. In the case of lower fluid temperatures, there are no major differences between the materials, although SS displays the fastest kinetics, which could be explained by the higher wall temperature. Furthermore, the fouling curve of the untreated polymer composite (C143-dg) seems to change to a steady state after 60 hours, whereas SS still shows a very steep increase. At this point, SS exhibits a fouling resistance value that is twice to three times higher than that of the polymer composites. To assess with certainty whether the differences between the materials are only due to the different wall temperatures or to the different surface properties, very long experiments or experiments at higher temperatures are necessary.

The results for higher fluid temperatures are more impressive. These are accompanied by higher wall temperatures, resulting in higher supersaturation and through the strongly temperature dependent surface integration of ions into the crystal lattice, an overall increase in the rate of crystal deposition [18,19].
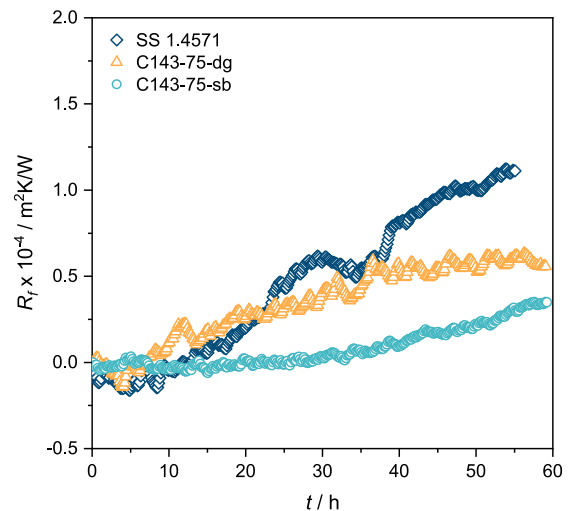

Figure 7: Fouling resistance curves. Exp. 1,3,4.

Especially on the SS surface, a sharp increase of the fouling resistance takes place in a short time, which speaks for fast kinetics compared to the polymer materials. Again, higher surface temperatures are obviously present on the SS surface, but this is compensated by the formation of the thick fouling layer on stainless steel during the experiment. An increasing fouling layer thickness causes the temperature to decrease at the fluid-fouling layer interface. Additionally, the fouling kinetics on stainless steel at a wall temperature of 68.9°C (Exp. 1). is faster than that on the polymer composite at a wall temperature of 71.1°C (Exp. 7). Thus, even when wall temperatures are considered, it is concluded that the polymer composites are less susceptible to fouling than stainless steel. Furthermore, it is remarkable that the untreated polymer is hardly affected by the higher temperatures, which are associated with higher supersaturations at the wall and hence faster kinetics. The reason for this is the poor adhesion of the salts to the surface, an effect which has already been demonstrated in the literature for polymer surfaces [20]. After reaching a critical layer thickness, this leads to parts of the fouling layer falling off, caused by the shear forces of the fluid flow (see t=47 h).
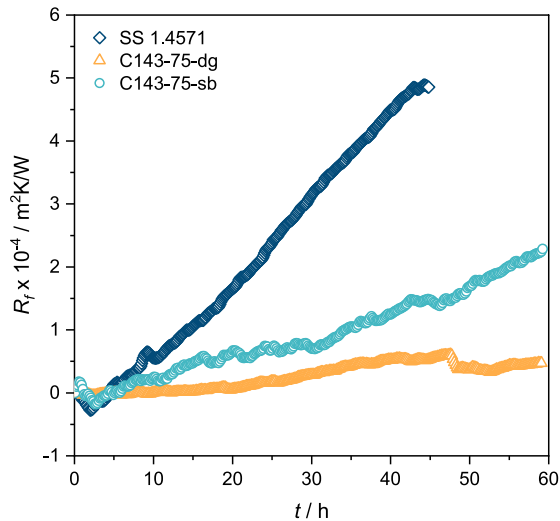
Figure 8: Fouling resistance curves. Exp. 5,7,8.

Figure 9: Fouling resistance curves. Exp. 9,10.

Incidentally, this also applies if a very large salt layer forms on the polymer composite sample due to bubble formation (as in Figure 5). The layer detached itself completely after drying and was only held in place by the walls of the heat exchanger. Cleaning in place of the materials with respect to crystallization fouling should therefore be straightforward based on the qualitative results shown here.

The fact that the sandblasted sample performed worse than the untreated sample at the higher fluid temperatures appears to be due to a change in induction phase, which decreases with increasing wall temperature due to increased crystallization fouling rates. The induction time is about 30 hours long for the lower temperatures (see Figure 7). Thereafter, the fouling kinetics exceed that of the untreated polymer.

In any case, the use of polymer composites seems to be advantageous over SS in systems susceptible to crystallization fouling. This is confirmed by the results with HX2 for calcium sulfate as well as for calcium carbonate fouling (Figure 9 and Figure 10 respectively). Even though the volume flow rates of the cold fluid streams were adjusted to give the same mean Reynolds numbers, different flow conditions prevail in this heat exchanger, as described in the materials and methods section. Thus, higher flow velocities than implied by the Reynolds number prevail there partially. This primarily leads to better removal of bubbles due to local turbulence. The improved removal also influences deposits, which, based on the previous discussion, mainly advantages the polymer composite.
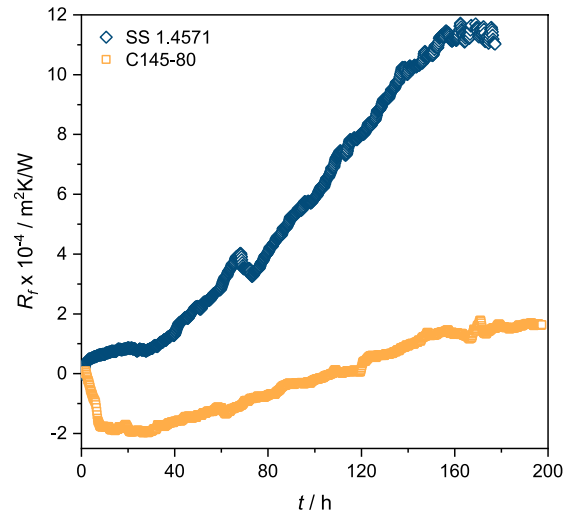
Figures 9 and 10 confirm this thesis. For both calcium sulfate and calcium carbonate, significantly higher fouling resistances are formed with SS as heat transfer surface. In addition, the polymer composite shows a strongly pronounced negative fouling resistance over a long period of time. Such negative fouling resistances result from increasing heat transfer coefficients due to local turbulence caused by initial crystal formation. Due to the poor adhesion to the composite, a covering fouling layer is never formed in HX2. It remains patchy, which explains the positive effect on the fouling resistance. The increased heat transfer coefficient thus almost compensates for (Figure 9) or exceeds (Figure 10) the thermal resistance caused by the deposits. This is also demonstrated by the amounts deposited on the surfaces in Table 3. The deposited quantities on the polymer composites are out of proportion to the low fouling resistances.

Table 3: Fouling quantity formed in HX2.

Exp. Nr.	Salt	m_{dep} / g/m²
9	$CaSO_4$	836.8
10	$CaSO_4$	163.7
11	$CaCO_3$	90.8
12	$CaCO_3$	19.9

Possible explanations for the results shown, which are frequently mentioned in the literature [21], are different energetic and topographic properties of the investigated materials. Since both the roughness and the energetic properties of the investigated materials differ, a sophisticated analysis proves to be difficult. Nevertheless, an attempt will be made to explain the results based on the aforementioned material properties. The mean arithmetic roughness, the surface free energies and the wettability with water of the materials and salts used are presented in Table 4.

Table 4: Material surface properties.

Material	γ_s / mNm	θ_{H_2O} / °	S_a / µm
SS 1.4571	40.46	81.4	0.077
C143-75	27.77	93.4	0.243
C143-sb	51.91	139.9	9.792
C145-80	27.83	92.2	0.703
$CaCO_3$ [22]	57.05	-	-
$CaSO_4$ [23]	47.88	-	-

A high surface roughness, usually leading to a shorter induction phase due to faster nucleation processes, does not seem to be crucial for the materials investigated. The reason for this assumption is the higher roughness of the composite material compared to SS. In addition, the roughest material investigated (C143-75-sb) shows the longest induction phase (see Figure 7). However, one effect that arises from the higher roughness is the stronger adhesion of the deposits. These did not simply fall off after drying of the fouled sandblasted surface as occurred in the case of the untreated composite. The advantage over SS in terms of lower asymptotic fouling resistance and slower crystallization fouling kinetics must therefore be due to the different surface free energies of the materials investigated.

Both scaling quantities and induction periods are strongly dependent on the interfacial energy differences between crystal and surface [24]. Smaller differences between the surface free energies of surface and crystal result in higher scaling susceptibility. A comparison of the surface free energies of the crystals and the materials studied (see Table 4) shows that the untreated polymer has advantages based on the conclusion drawn earlier, which is consistent with the experimental results. This may also provide an explanation regarding the higher fouling tendency of the materials with $CaSO_4$ since the interfacial energy difference between crystal and heat transfer surface is found to be lower for this test system.
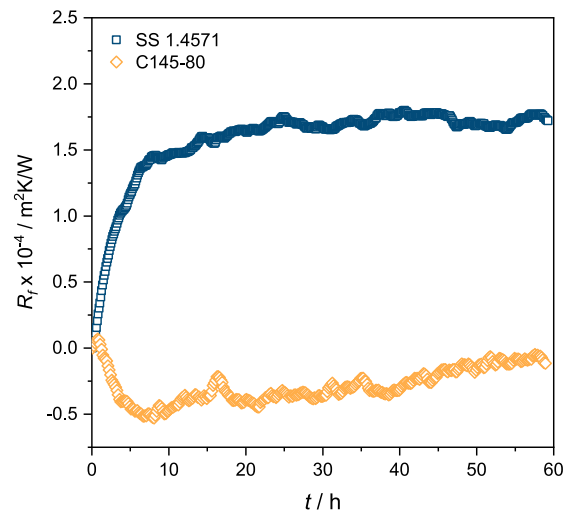

Figure 10: Fouling resistance curves. Exp. 11,12.

According to this theory, the sandblasted sample should have the highest fouling susceptibility, which could not be confirmed. The reason for this inconsistency in the results lies in the method of determining the surface free energy. This was performed with the OWRK method using optical contact angle measurements. However, the underlying Young's equation is only valid for perfectly smooth surfaces [25]. Yet an increase in roughness leads to an increase in the contact angle for liquids that have a contact angle >90 ° on the smooth surface and vice versa [26]. As a result, the sandblasting of the materials apparently increases the surface free energy. The actual value, of course, should be the same as that of the non-sandblasted sample, which is in accordance with the experimental results.

CONCLUSION

The use of the fabricated highly filled polypropylene/graphite composites in systems susceptible to crystallization fouling resulted in significantly reduced fouling proneness compared to stainless steel (SS) when bubble formation was avoided. This was shown by slower crystallization kinetics and the formation of lower fouling quantities, for both model salts investigated. Due to lower thermal conductivities of the polymer composites, the use of SS provides higher heat transfer rates, but this fact can be reversed by the formation of larger fouling layers on the metal.

Avoiding the formation of bubbles by means of adapted heat exchanger geometries represents a particularly promising possibility in this context. In plate heat exchangers with corrugation patterns, for example, this should be completely prevented by the turbulence present. However, the verification of this assumption is still pending and needs to be verified in following studies.

Another major advantage is the low adhesion of deposits to the composite materials, which leads to a self-cleaning effect that could reduce downtimes for

cleaning in technical processes. Again, the classic design of the plate heat exchanger could therefore be advantageous.

The resistance to corrosive media and the reduced susceptibility to fouling already make the developed materials a suitable alternative to metallic materials.

ACKNOWLEDGEMENTS

NOMENCLATURE

A	Heat transfer surface, m^2
B	Bias uncertainty, dimensionless
b	Molality, mmol/kg
c_p	Specific heat at constant pressure, J/kgK
h	Convective heat transfer coefficient, W/m²K
L	Length, m
$\dot{m}$	Mass flow rate, kg/s
m_{dep}	Deposited mass per area, g/m²
$\dot{Q}$	Heat transfer rate, W
R_f	Fouling resistance, (m²K)/W
Re	Reynolds number, dimensionless
S_a	Mean arithmetic surface roughness, μm
t	time, h
T	Temperature, °C
U	Overall heat transfer coefficient, W/(m²K)
w	Heat exchanger width, m
x	Heat exchanger length, m

Special characters

γ	Free surface energy, mN/m
ΔT_{lm}	Mean log Temperature difference, K
θ	Contact angle, °

Subscripts

b	Bubble
c	Cold fluid conditions
calc	Calculated
h	Hot fluid conditions
in	Inlet conditions
f	Fouled surface
l	Liquid conditions
out	Outlet conditions
s	Solid properties
w	Conditions at the wall
0	Initial conditions

Abbreviations

dg	Degassed
HX	Heat exchanger
Sb	Sandblasted
SS	Stainless steel

REFERENCES

[1] T. Lestina, Heat Exchangers Fouling, Cleaning and Maintenance, in: F.A. Kulacki (Ed.), Handbook of Thermal Science and Engineering, Springer International Publishing, Cham, 2017, pp. 1–33.

[2] R. Steinhagen, H. Müller-Steinhagen, K. Maani, Problems and Costs due to Heat Exchanger Fouling in New Zealand Industries, Heat Transfer Engineering 14 (1993) 19–30.

[3] S. Kakaç, H. Liu, A. Pramuanjaroenkij, Heat Exchangers, CRC Press, 2020.

[4] C. T'Joen, Y. Park, Q. Wang, A. Sommers, X. Han, A. Jacobi, A review on polymer heat exchangers for HVAC&R applications, International Journal of Refrigeration 32 (2009) 763–779.

[5] O. Breuer, U. Sundararaj, Big returns from small fibers: A review of polymer/carbon nanotube composites, Polym Compos 25 (2004) 630–645.

[6] X. Chen, Y. Su, D. Reay, S. Riffat, Recent research developments in polymer heat exchangers – A review, Renewable and Sustainable Energy Reviews 60 (2016) 1367–1386.

[7] P. Sobolčiak, A. Abdulgader, M. Mrlik, A. Popelka, A. A Abdala, A. A Aboukhlewa, M. Karkri, H. Kiepfer, H.-J. Bart, I. Krupa, Thermally Conductive Polyethylene/Expanded Graphite Composites as Heat Transfer Surface: Mechanical, Thermo-Physical and Surface Behavior, Polymers 12 (2020).

[8] N. Andritsos, A. Karabelas, Calcium carbonate scaling in a plate heat exchanger in the presence of particles, International Journal of Heat and Mass Transfer 46 (2003) 4613–4627.

[9] H. Kiepfer, P. Stannek, M. Kuypers, M. Grundler, H.-J. Bart, Highly Conductive Thin-Walled Polypropylene/Graphite Composites as Heat Transfer Surfaces in Corrosive Media, in: HEFAT (Ed.), Proceedings of the 15th International Conference on Heat Transfer, Fluid Mechanics and Thermodynamics (HEFAT2021), 2021, pp. 1174–1179.

[10] D.H. Kaelble, Dispersion-Polar Surface Tension Properties of Organic Solids, The Journal of Adhesion 2 (1970) 66–81.

[11] D.K. Owens, R.C. Wendt, Estimation of the surface free energy of polymers, J. Appl. Polym. Sci. 13 (1969) 1741–1747.

[12] M. Mortean, M. Mantelli, Nusselt number correlation for compact heat exchangers in transition regimes, Applied Thermal Engineering 151 (2019) 514–522.

[13] H.D. Baehr, K. Stephan, Konvektiver Wärme- und Stoffübergang. Einphasige Strömungen, in: H.D. Baehr, K. Stephan (Eds.), Wärme- und Stoffübertragung, Springer Berlin Heidelberg, Berlin, Heidelberg, 2019, pp. 313–501.

[14] W.L. Ryan, E.A. Hemmingsen, Bubble Formation in Water at Smooth Hydrophobic Surfaces, Journal of Colloid and Interface Science 157 (1993) 312–317.

[15] Ryan, Hemmingsen, Bubble Formation at Porous Hydrophobic Surfaces, Journal of Colloid and Interface Science 197 (1998) 101–107.

[16] P. Roach, N.J. Shirtcliffe, M.I. Newton, Progess in superhydrophobic surface development, Soft matter 4 (2008) 224–240.

[17] S.M. Peyghambarzadeh, A. Vatani, M. Jamialahmadi, Influences of bubble formation on different types of heat exchanger fouling, Applied Thermal Engineering 50 (2013) 848–856.

[18] T.R. Bott, Aspects of crystallization fouling, Experimental Thermal and Fluid Science 14 (1997) 356–360.

[19] T.M. Pääkkönen, M. Riihimäki, C.J. Simonson, E. Muurinen, R.L. Keiski, Crystallization fouling of CaCO3 – Analysis of experimental thermal resistance and its uncertainty, International Journal of Heat and Mass Transfer 55 (2012) 6927–6937.

[20] H. Kiepfer, W. Omar, T. Schröder, H.-J. Bart, Polymer Film Heat Transfer Surfaces in Seawater Desalination: Fouling Layer Formation and Technology, Chem. Eng. Technol. 43 (2020) 1205–1213.

[21] W. Augustin, J. Zhang, I. Bialuch, T. Geddert, S. Scholl, Modifizierte Oberflächenbeschichtungen zur Foulingminderung auf wärmeübertragenden Flächen, Chemie Ingenieur Technik 78 (2006) 607–612.

[22] A. Calhoun, E. Chiang, Determination of the surface energetics of surface modified calcium carbonate using inverse gas chromatography, J Vinyl Addit Technol 12 (2006) 174–182.

[23] M. Förster, W. Augustin, M. Bohnet, Influence of the adhesion force crystal/heat exchanger surface on fouling mitigation, Chemical Engineering and Processing: Process Intensification 38 (1999) 449–461.

[24] C. Dreiser, L.J. Krätz, H.-J. Bart, Kinetics and Quantity of Crystallization Fouling on Polymer Surfaces: Impact of Surface Characteristics and Process Conditions, Heat Transfer Engineering 36 (2015) 715–720.

[25] P.C. Zielke, Experimental investigation of the motion of droplets on surfaces with a gradient in wettability, PhD thesis, Friedrich-Alexander-Universität Erlangen-Nürnberg, Erlangen-Nürnberg, 2008.

[26] D. Quéré, Wetting and Roughness, Annu. Rev. Mater. Res. 38 (2008) 71–99.